JOURNAL OF CATALYSIS 56, 198–218 (1979)

Morphology and Composition of Pt–Pd Alloy Crystallites on SiO_2 in Reactive Atmospheres[1]

M. CHEN AND L. D. SCHMIDT

Department of Chemical Engineering and Materials Science, University of Minnesota, Minneapolis, Minnesota 55455

Received July 7, 1978; accepted September 19, 1978

Scanning transmission electron microscopy and energy dispersive X-ray microanalysis are used to examine the structure, sintering rates, and chemical composition of 20 to 200-Å-diameter Pt–Pd alloy crystallites on planar amorphous SiO_2. Oxygen causes Pt-Pd alloy crystallites to separate into distinct crystallites of metal and tetragonal PdO, both of which are in contact with the SiO_2 support. Oxide is first observed at 300 to 400°C depending on composition, and the oxide begins to decompose at 650°C and completely disappears between 740 and 850°C. For high Pt alloys the oxide nucleates and grows at one side of the metal particles but for high Pd alloys small (20 to 40 Å) Pt particles form around the edges of the PdO crystal. The oxide can be reduced by H_2 even at room temperature, and this produces distinct and separated Pt and Pd-rich particles as shown by single particle microanalysis. These morphologies are presumably caused by stronger interfacial interactions between PdO and SiO_2 compared to that between metal and the oxides. A stability diagram for formation of oxide shows that oxide is formed only for alloys containing at least 15% Pd. Evaporation of Pt as PtO_2 is inhibited by the presence of Pd, and growth of crystallites is slower for alloys than for pure Pt metal. Implications of these results on the structures of supported alloy catalysts will be discussed.

INTRODUCTION

Supported metal catalysts are exposed to various oxidizing and reducing gas atmospheres during their preparation, operation, and regeneration, and interaction with these gases can have profound effects on catalyst morphology and sintering rates (*1*, *2*). Even though Pt forms no bulk oxides, there is indirect evidence for surface oxide formation (*3*). However, no direct evidence for oxides on Pt catalysts has been noted by microscopic examination or in X-ray or electron diffraction (*1*, *2*). On the other hand, Pd readily forms a tetragonal bulk oxide PdO upon heating Pd films to 300°C, and other less stable oxides have been identified (*4*, *5*). There is considerable evidence that Pd and Pt–Pd supported on SiO_2 or Al_2O_3 can be prepared in either metal or oxide forms and that its catalytic properties are strongly affected by such treatment (*5–8*).

Alloy catalysts should be even more strongly influenced by exposure to oxygen because the components in alloys have different oxide-forming properties. It has been shown that exposure of alloys such as Ni–Au (*9*), Cu–Ni (*10*), and Pd–Au (*11*) to O_2 produces a surface enrichment of one species as its oxide. Such enrichment phenomena cannot occur to the same extent in sufficiently small crystallites because only a finite bulk reservoir exists.

[1] This work partially supported by NSF under Grant No. ENG75-01918.

0021-9517/79/020198-21$02.00/0

However, small crystallites possess additional possibilities regarding phase separation and morphologies.

We report observations of the effects of heating Pt–Pd alloys and Pd on a planar amorphous SiO_2 substrate in air, N_2, and H_2. These experiments are analogous to those reported previously for Pt on SiO_2 (*1*). Even though the Pt–Pd phase diagram predicts complete solid solutions, quite different and distinctive morphologies are observed which are due to the formation and decomposition of PdO.

EXPERIMENTAL

Apparatus and procedures have been described in a previous paper (*1*). A thin ($\leq$500-Å) planar substrate of amorphous SiO_2 was prepared by air oxidation at 1100°C of a (111) Si specimen which had been thinned by HNO_3 and HF jet etching and argon ion micromilling. Pt and Pd were deposited sequentially by vacuum evaporation with total initial film thickness typically 10 to 25 Å as estimated by weight loss of Pt and Pd foils on tungsten evaporation sources. From the accuracy of weight measurement we estimate compositions to be accurate to within a few percent and total film thicknesses within $\pm$5 Å. Compositions of alloys will be designated as *atomic* percent of Pd. After deposition, the specimens were vacuum annealed to 450°C for 3 hr to bring the alloys to equilibrium and produce small crystallites 10 to 20 Å in diameter. To compare pure Pt with alloys accurately, one-half of the SiO_2 specimen was masked during Pd deposition in some experiments so that regions with different composition could be exposed to gases for identical temperature and times. Samples were heated for known times and temperatures in a 3-cm-diameter quartz tube in gases at 1 atm with flow rates of $\sim$0.5 cm^3/sec. High purity gases were used without further purification.

Specimens were transferred to a JEOL JEM-100C scanning transmission microscope for observation. This instrument had a resolution of 3.4 Å in TEM with an electron beam size of 15 Å in the STEM mode for energy dispersive X-ray analysis and electron microdiffraction. While specimens were exposed to laboratory air, they were self-supporting and were not treated or exposed to liquids after their preparation. No evidence of contamination was noted in any experiments. Scanning Auger microanalysis and X-ray microanalysis of some specimens indicated no detectable impurities, although of course the presence of monolayer amounts of various contaminants such as carbon cannot be eliminated. In time–temperature experiments the same specimen was transferred repeatedly between heating tube and microscope so that each composition represents observations on a single region of a single specimen.

RESULTS

Structure of 50% Pd Alloy

Specimens with 50% Pd at an initial total film thickness of $\sim$10 Å were heated in air between 300 and 900°C. Electron diffraction and morphology indicated that the particles formed at 310°C for 1 hr were exclusively FCC metal. However, after heating to 415°C for 1 hr, both FCC and PdO phases were observed by electron diffraction. As shown in Fig. 1a, microscopic observation also indicated the presence of irregularly shaped lower contrast particles in addition to the typical metal crystallites. The size and number of these PdO particles increased as the temperature was increased. Metal particles decreased in number and increased in size, although, as will be discussed later, metal loss rates appeared to be considerably inhibited compared with pure Pt. At 615°C particles are somewhat larger and oxide particles are well developed, either as isolated crystallites or as crystallites growing at the side of metal crystallites as shown in Fig. 1b.

After heating to 750°C for 1 hr, particle size increased significantly, all particles

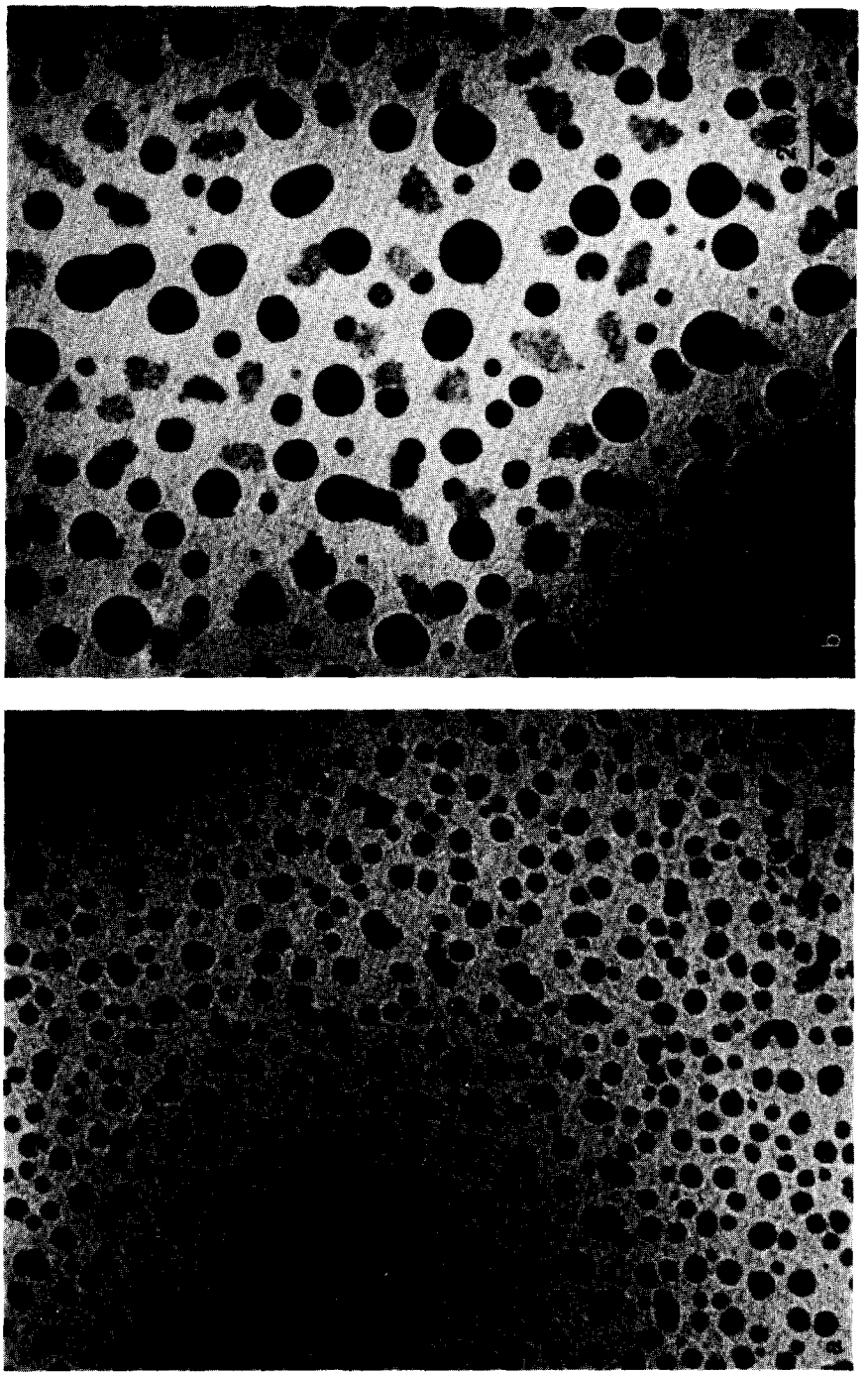

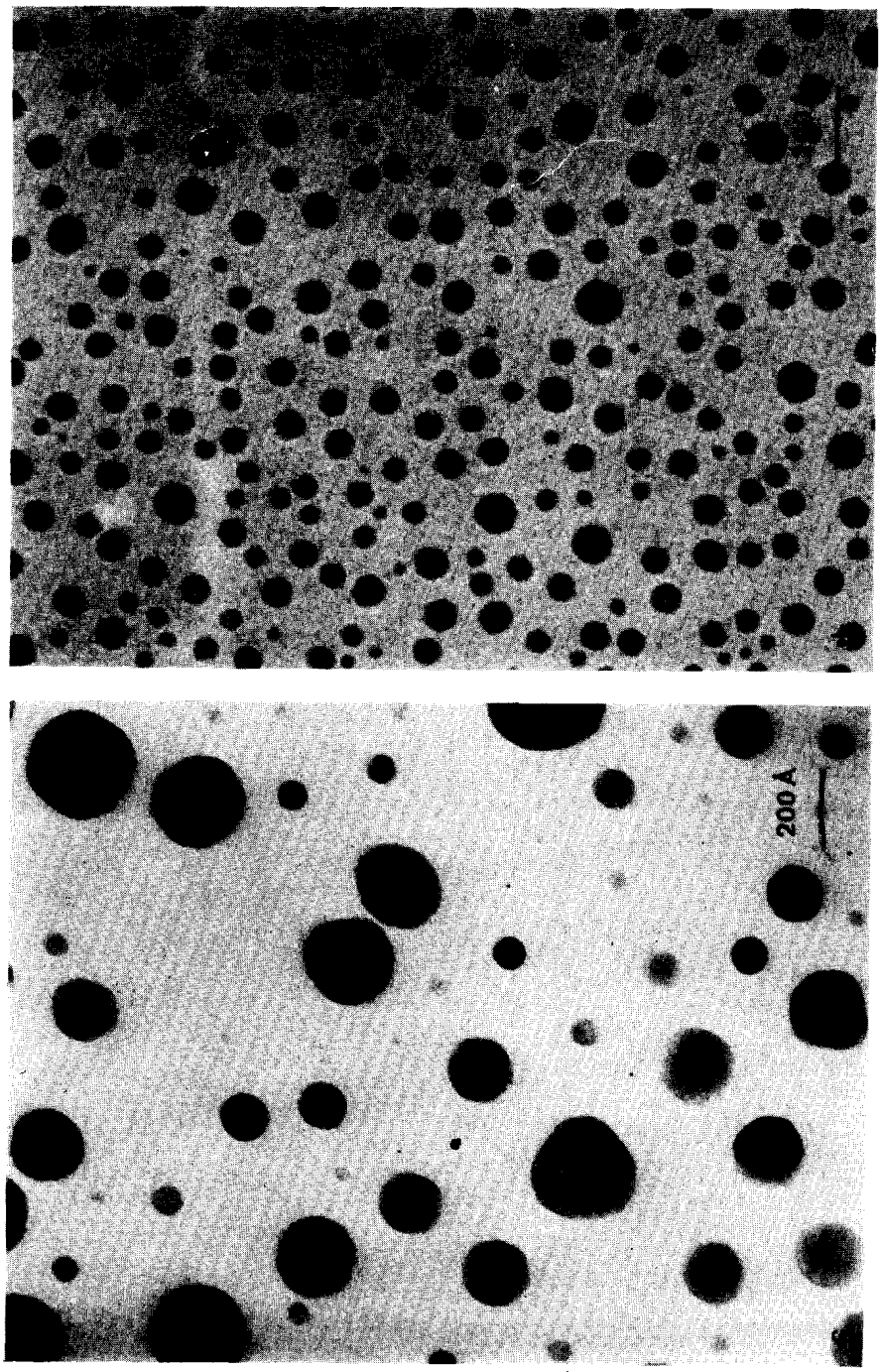

FIG. 1. Micrographs of 50% Pd alloy on amorphous SiO_2 after heating in air for 1 hr at temperature of (a) 415°C, (b) 615°C, and (c) 750°C. (d) shows a specimen with an identical metal loading and composition after heating in N_2 for 1 hr at 600°C. (a) and (b) exhibit characteristic oxide particles formed in air below 700°C, while (d) shows that particle growth is much slower in N_2 than in air.

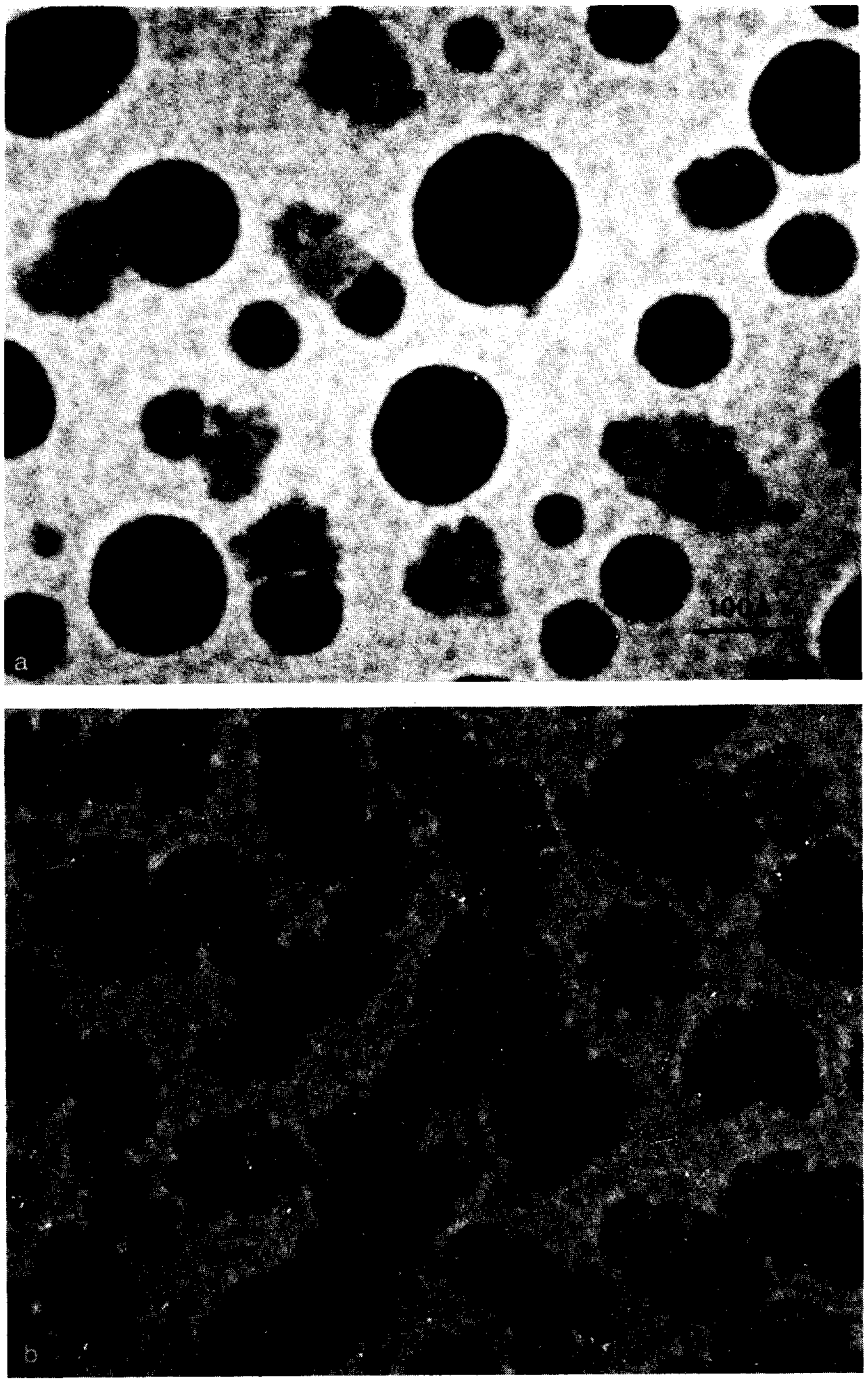

FIG. 2. High magnification micrograph of alloys heated in air at 615°C. (a) shows a 50% alloy with characteristic PdO crystallites nucleated at the edge of metal crystallites. (b) shows the small Pt particles (~20 Å) which form at the edge of PdO crystallites for an alloy containing ~95% Pd.

appeared metallic, and only the FCC structure was observed as shown in Fig. 1c. This is consistent with the decomposition temperature reported for PdO (*4*).

The difference in morphology between PdO and FCC particles is illustrated at higher magnification in Fig. 2a. Oxide particles have irregular shapes and lower contrast compared to metal particles. The low contrast of PdO appears to be due to two effects, the low average atomic scattering factor of PdO compared with that of Pt and an improved "wetting" or contact of PdO on SiO_2 which results in thinner oxide particles than for metal particles. This will be discussed later.

Figure 1d shows the morphology and diffraction pattern of a 50% Pd specimen which was heated in N_2 at 600°C for 1 hr. Neither PdO diffraction lines nor nonmetallic crystallites were observed. When heated in N_2, the alloy particles retained the FCC structure at all temperatures up to at least 900°C.

Structure of Pure Pd

When a specimen with an initial Pd film thickness of ~15 Å was heated in air to 305°C for 1 hr the electron diffraction pattern showed only the tetragonal structure of PdO. Further heating up to 700°C did not produce any significant change in morphology or size of particles. Figure 3 shows the morphology and diffraction pattern of PdO after heating at various temperature between 300 and 900°C. Decomposition of PdO began above 740°C and was completed by 850°C. Figure 3d shows the shapes of particles after heating at 850°C for 1 hr. In order to suppress oxide reformation during cooling in these experiments, N_2 gas was substituted for air after the specimen had been heated at 850°C for 1 hr so that the specimen cooled to room temperature in N_2. The average particle size and number of Pd particles left on SiO_2 was estimated from Fig. 3d to be 690 Å and $7.5 \times 10^8/cm^2$, respectively.

Structure of Pd-Rich Alloys

A specimen of 77% Pd with an initial film thickness of 20 Å was heated in air between 300 and 900°C. At 305°C, the diffraction pattern showed only the FCC structure, but the oxide was observed at 400°C. When the PdO formed, microcrystallites of Pt about 40 Å in diameter were observed to be expelled out of each PdO particle and to be located at the edge of Pdo crystallites as shown in Figs. 4a and 2b. Further heating of the specimen up to 700°C did not result in a significant change of morphology or sizes of either metal or oxide particles. The observed decomposition temperature was approximately the same as for the pure Pd specimen. Figure 4d shows the morphology of particles after heating to 850°C with N_2 added during cooling to suppress low temperature oxidation. The number and average size of the particles left on SiO_2 after 850°C treatment were about $1.4 \times 10^{10}/cm^2$ and 280 Å, respectively. These numbers are quite different from those obtained for pure Pd specimen in that alloy specimens yield larger numbers and smaller sized Pd particles. Thus, the addition of a small amount of Pt results in much reduced sintering compared to pure Pd when heated in air. Comparison of pure Pd and the alloy containing a small amount of Pt was made on separate specimens and also with both compositions on a single specimen. Results were qualitatively similar. The reduced sintering in Pd-rich alloy may be caused by the presence of small Pt particles on specimen prior to decomposition which serve as nuclei for Pd formed by oxide decomposition.

Partial Oxidation

The effect of reoxidation during cooling on the morphology of particles was examined for a specimen with 95% Pd. The

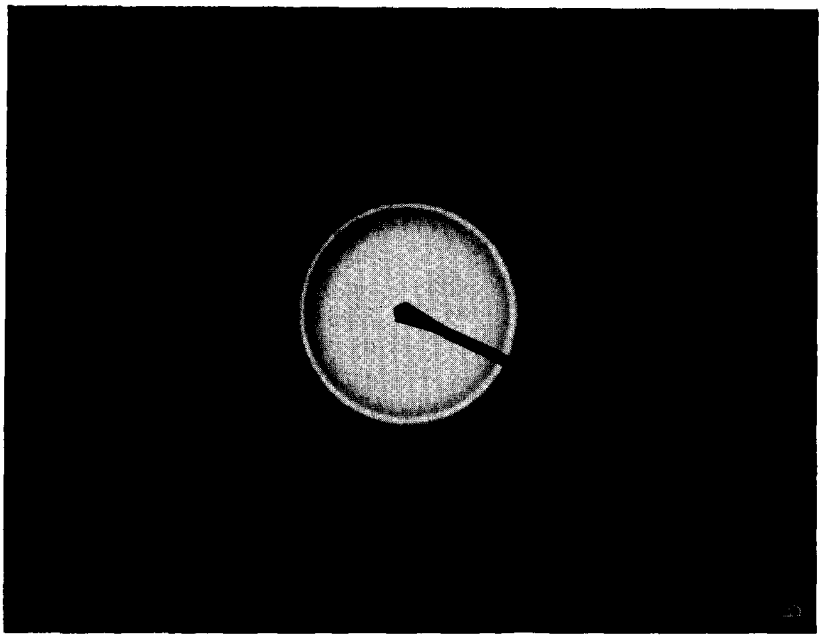

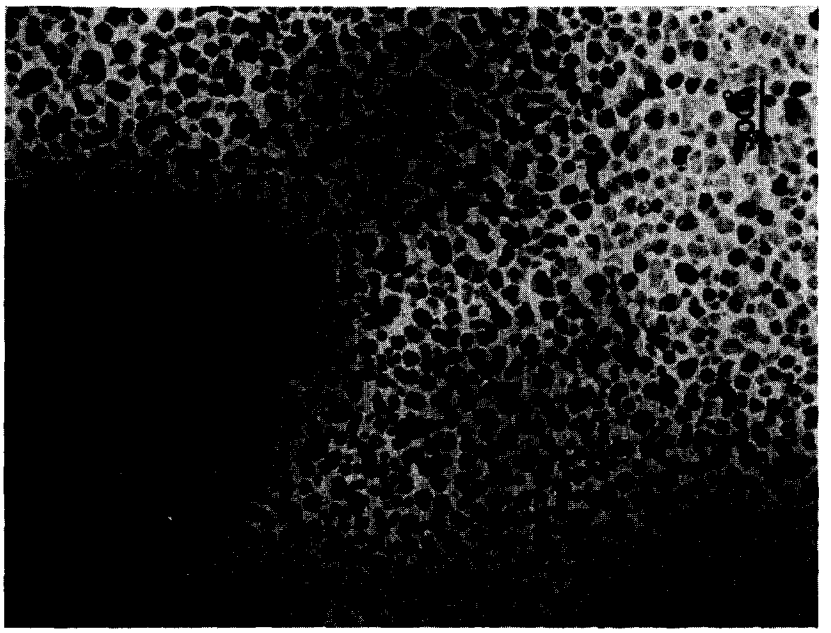

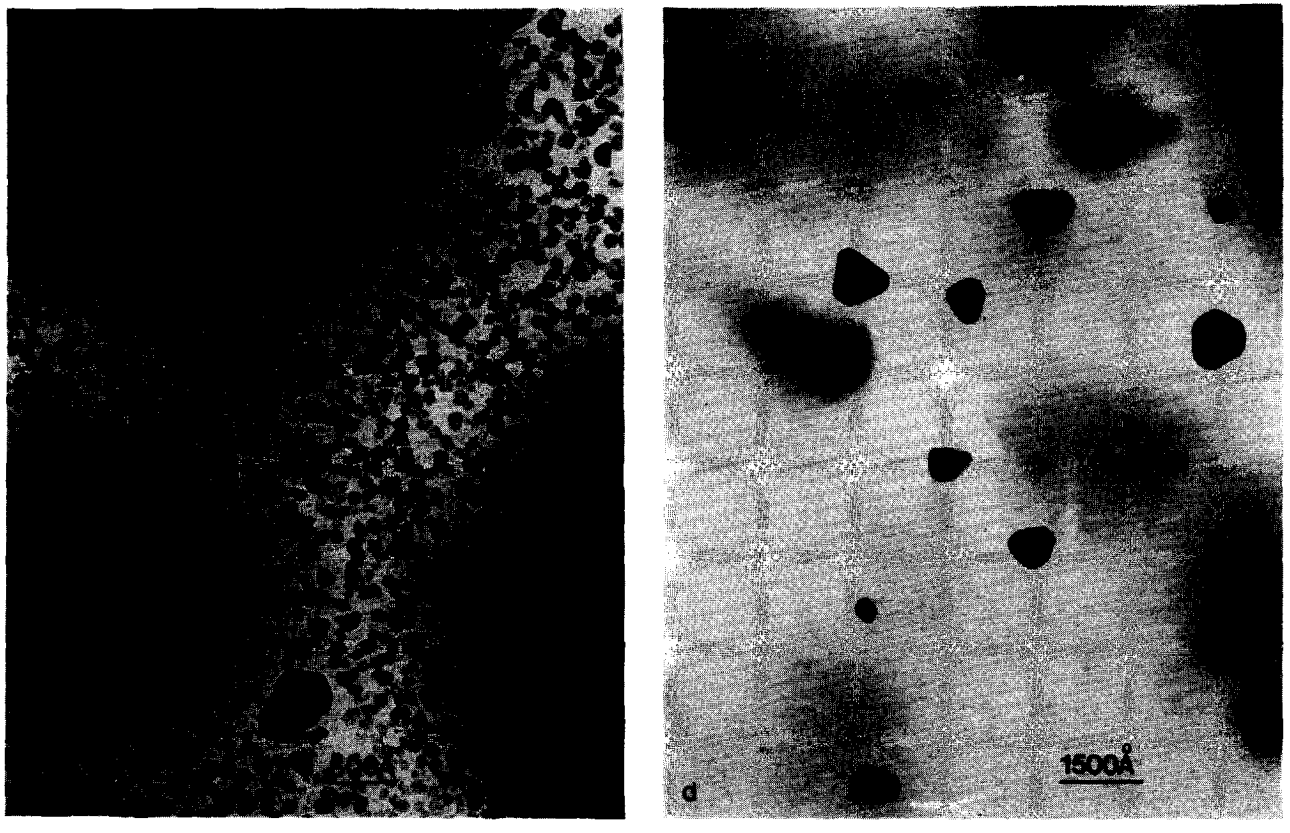

FIG. 3. Pure Pd after heating for 1 hr in air at (a) 400°C, (b) 775°C, and (d) 850°C. (b) shows the electron diffraction pattern of (a) which shows that at 30°C all of the Pd had been oxidized to tetragonal PdO. (c) exhibits several large particles characteristic of rapid growth which accompanies oxide decomposition.

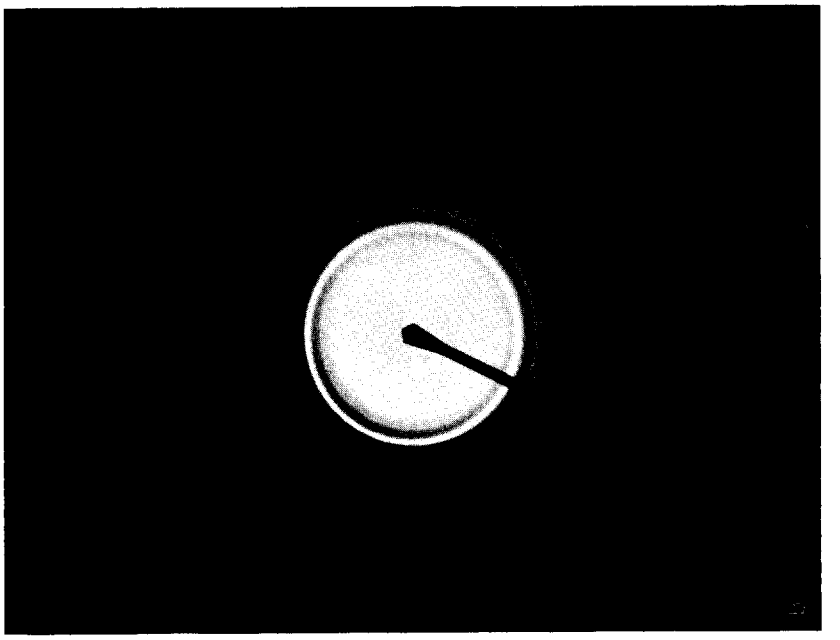

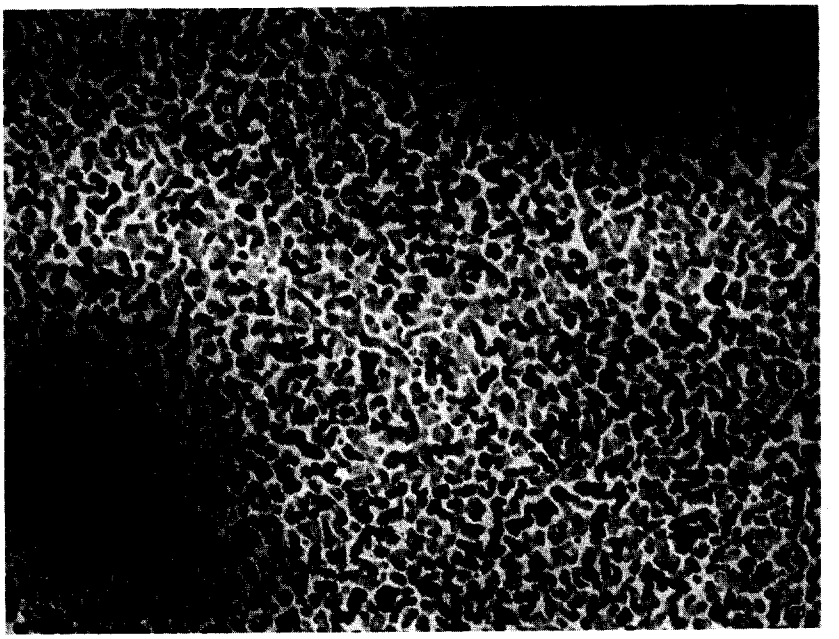

FIG. 4. Micrographs of a 77% Pd alloy after heating in air for 1 hr to (a) 400°C, (b) 775°C, and (d) 850°C. (b) shows the electron diffraction pattern of (a) which exhibits both fcc rings of metal (particle size ~40 Å) and tetragonal rings of PdO. (c) shows several large metal particles characteristic of rapid growth accompanying oxide decomposition as also seen in pure Pd (Fig. 3c).

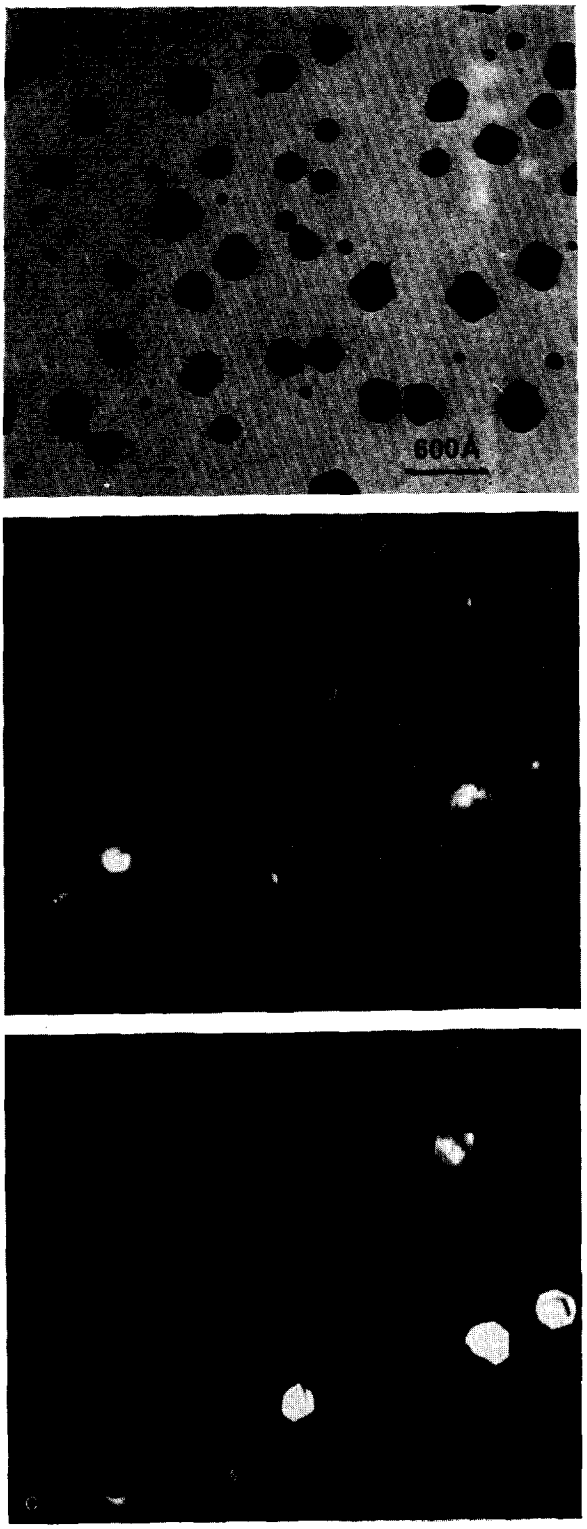
600Å

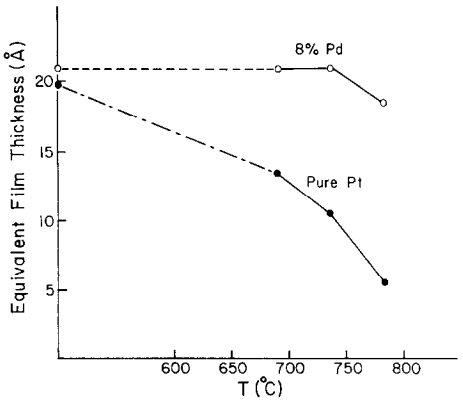

FIG. 6. Figure showing enhanced evaporation of pure Pt (solid circles) compared to 8% Pd (open circles). Equivalent film thickness was estimated by measuring particle density and average diameter assuming particles were hemispheres.

specimen was heated up to 850°C and then cooled to room temperature in air. (Cooling to 300°C required approximately 2 min.) Figure 5 shows the morphology of the particles. The shapes of the resulting particles were substantially different from those obtained by N_2 treatment, probably due to oxide formation during cooling.

Dark field microscopy was used to identify location of PdO phases in these experiments. Figures 5a, b, and c show bright field and dark field images of the same particles. Since the reflection of PdO in dark field shows only a portion of each particle, it appears that a layer or skin of microcrystalline PdO oxide is formed on top of FCC particles by this treatment.

Structure of Pt-Rich Alloys and Metal Volatilization

When specimens with compositions of 8 or 12% Pd were heated in air, no evidences of oxide were noted from electron diffraction or micrographs for all temperatures between 300 and 800°C.

Pure Pt crystallites have been observed to evaporate as PtO_2 when heated in air above 700°C. However, PdO has negligible vapor pressure even at very high temperatures (*12*). The vapor pressure of pure Pd is also considerably lower than that of PtO_2 (*13*). The relative metal loss rates of pure Pt and Pt-rich alloys were compared by preparing a specimen on which one-half was pure Pt and the other half contained 8% Pd (both halves had the same amount of Pt so the alloy region had a slightly higher total metal loading). The initial film thickness were about 20 and 22 Å for pure Pt and Pt-rich regions, respectively. The amount of metal remaining (equivalent film thickness) versus temperature for heating times of 1 hr was estimated from micrographs assuming the particles attained hemispherical shape. From this the equivalent film thickness t of the film at each temperature was calculated using the equation $t = v/A$ where v is the total volume of metal calculated and A is the area analyzed. Figure 6 shows the equivalent film thickness versus temperature for both regions. It is evident that a much higher rate of metal loss occurs on the pure Pt region than on the 8% Pd alloy.

Oxide Stability Diagram

Similar experiments were repeated for alloys with different compositions. The phases in each observation, identified by electron diffraction and micrographs, are indicated by points in Fig. 7. For each point shown the specimen was heated at the temperature indicated for 1 hr. The maximum Pd composition in which no PdO is observed at any temperature is estimated as 15%. The maximum possible amount of oxide is of course proportional to the initial amount of Pd, and the presence of oxide becomes more difficult to detect for Pt-rich alloys. However, the

FIG. 5. Micrographs of large (~400-Å-diameter) 95% Pd particles illustrating partial oxidation. Specimens were heated to 850°C in air to form large metal crystallites and then cooled in air. (a) shows the bright field image, (b) the dark field image of the {002} and {101} diffraction rings of PdO and part of diffuse ring of SiO_2, and (c) the dark field image of the {111} and {200} diffraction rings of fcc.

sensitivity of oxide detection was such that only a few percent of crystalline oxide should have escaped detection in these experiments.

X-Ray Microanalysis of Individual Particles

The compositions of individual particles on the SiO_2 support after PdO decomposition were examined by energy dispersive X-ray analysis in the microscope. The minimum diameter analyzed is about 100 Å for point analysis. However, point analysis proved to be difficult because beam heating caused particles to move during analysis, presumably because of the low thermal conductivity of SiO_2. Therefore, we used the small area scan mode for X-ray analysis. The area analyzed was about 230 × 230 Å. In this mode, one could "see" the particle from its STEM image and adjust the scan area if the specimen moved. Note that the effective spatial resolution using this technique with a single particle is the particle size rather than the beam size. Counting rates were higher and statistics were improved for larger particles, and the minimum single particle size on which analysis was considered significant was actually ~100 Å. Table 1 shows the net counts (after substracting backgrounds for Pt and Pd peaks) and also the net count ratios of Pd/Pt. From these ratios, we found the individual particles showed composition variations by up to a factor of 4 although there appeared to be no pure Pt or Pd particles. Figure 8 shows micrographs of the particles analyzed. Figure 8a is the STEM micrograph and Figs. 8b and c the TEM micrograph of a region after and before PdO decomposition. The letters (a, b, c, ..., etc.) in the micrographs correspond to the particles listed in Table 1. From Fig. 8, it is seen that particles with lower Pd/Pt ratios in Table 1 correspond in general to the particles with less PdO near them before decomposition (particle l was an exception).

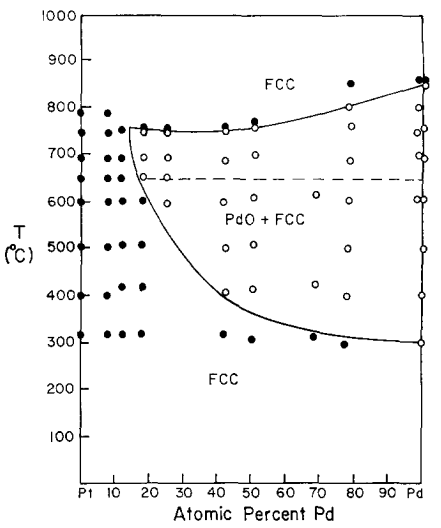

FIG. 7. Stability diagram showing phases observed following heating for 1 hr in air at temperatures indicated. Solid circles indicate conditions where only fcc was observed while open circles indicate where both fcc and PdO were observed. The dashed line indicates the temperature above which the amount of oxide began to decrease.

X-Ray microanalysis thus confirms the conclusion from morphology and diffraction that particles show composition variations after heat treatment in air.

TABLE 1

X-Ray Microanalysis of Individual Alloy Particles

Particle[a]	Pd[b]	Pt[c]	Pd/Pt
a	475	1090	0.44
b	571	1455	0.39
c	129	664	0.19
d	355	557	0.64
e	457	1340	0.34
f	198	1392	0.14
g	160	487	0.33
h	218	1542	0.14
i	420	982	0.43
j	295	560	0.53
k	520	1308	0.40
l	355	535	0.66

[a] Shown in Fig. 8.
[b] Pd, 2.525–3.593 keV.
[c] Pt, 9.135~9.779 keV.

Hydrogen Reduction

PdO particles could be reduced by H_2 even at room temperature (*4, 5, 14*). A specimen with 50% Pd was oxidized in air at 650°C for 1.5 hr. Figure 9a shows the characteristic morphology of the FCC and PdO phases as described previously. This specimen was then reduced in a stream of H_2 (1 atm, ~0.5 cm³/sec) at 23°C for 10 hr. The electron diffraction pattern showed that the PdO phase had disappeared entirely after reduction. Figure 9b shows the electron micrograph after reduction of the same area as in Fig. 9a. A comparison of Figs. 9a and b reveals that the FCC particles were not affected by exposing to H_2 gas at 23°C while PdO particles were reduced to metal and the resulting Pd particles had a *smaller apparent size* than those of corresponding PdO particles.

Diffraction Intensity and Line Broadening

The intensities and line widths of electron diffraction peaks of several samples were examined by microdensitometer scan of ring patterns. Figure 10 shows typical microdensitometer traces for Pt, alloy, and alloy with PdO. The intense broad peaks near the origin are from amorphous SiO_2 and all other peaks in all micrographs could be identified either with FCC metal or tetragonal PdO. In principle the metal alloy composition can be determined by measuring the lattice constant (*15*) of alloy samples. However, variations are small and we did not attempt to analyze metal composition by this method.

X-Ray line broadening has been used successfully in determining the average size and structure of supported metal catalyst particles (*16*), although particles smaller than 50 Å cannot generally be detected by X-ray diffraction. With electron diffraction one can typically detect particle size down to 20 Å and thus extend the range of line broadening measurement of crystallite size. Using the Debye–Scherrer equation

$$D = \lambda/[\theta^2(D) - \theta^2(D_\infty)]^{\frac{1}{2}} \qquad (1)$$

where $\theta(D)$ is the diffraction line width (full width at half maximum) of a crystal with size D and $\theta(D_\infty)$ is controlled by instrumental broadening. In this experiment $\theta(D_\infty)$, determined by measuring the line width of the (111) peak of a thin single crystal of silicon, was 3.59×10^{-4} rad. The average crystal size D was calculated from Eq. (1) by measuring the line width of the peaks. The average particle size $\bar{d}$ determined from electron micrographs was compared with the crystal size D. The solid curve in Fig. 11 represents the calculated crystallite size from Eq. (1) while data points represent the average particle sizes. Oxide particles were irregularly shaped and the average size was determined by cutting out micrographs and weighing them to determine areas. Geometrical and crystal sizes are seen to agree to within experimental error for Pt, alloys, and PdO. This shows that *particles are highly crystalline.* No effects of disorder or twinning were noted from diffraction line broadening. The difference in the average size measured by the two techniques may of course influence the comparison. In fact, electron line broadening provides a convenient and accurate method to determine the average size of particles less than 150 Å in diameter.

The growth rate of 50% Pd alloy heated in air was examined by measuring D and $\bar{d}$ for metal and oxide versus temperature as shown in Fig. 12a. As described previously, the size of PdO increased as the temperature was increased and PdO disappeared above 740°C. For metal particles the growth behavior is similar to that of pure Pt on SiO_2 (*1, 17*) for temperature below 700°C. There was an abrupt increase in size above 700°C in the alloy which is associated with the decomposition of PdO. The size distribution histograms of PdO

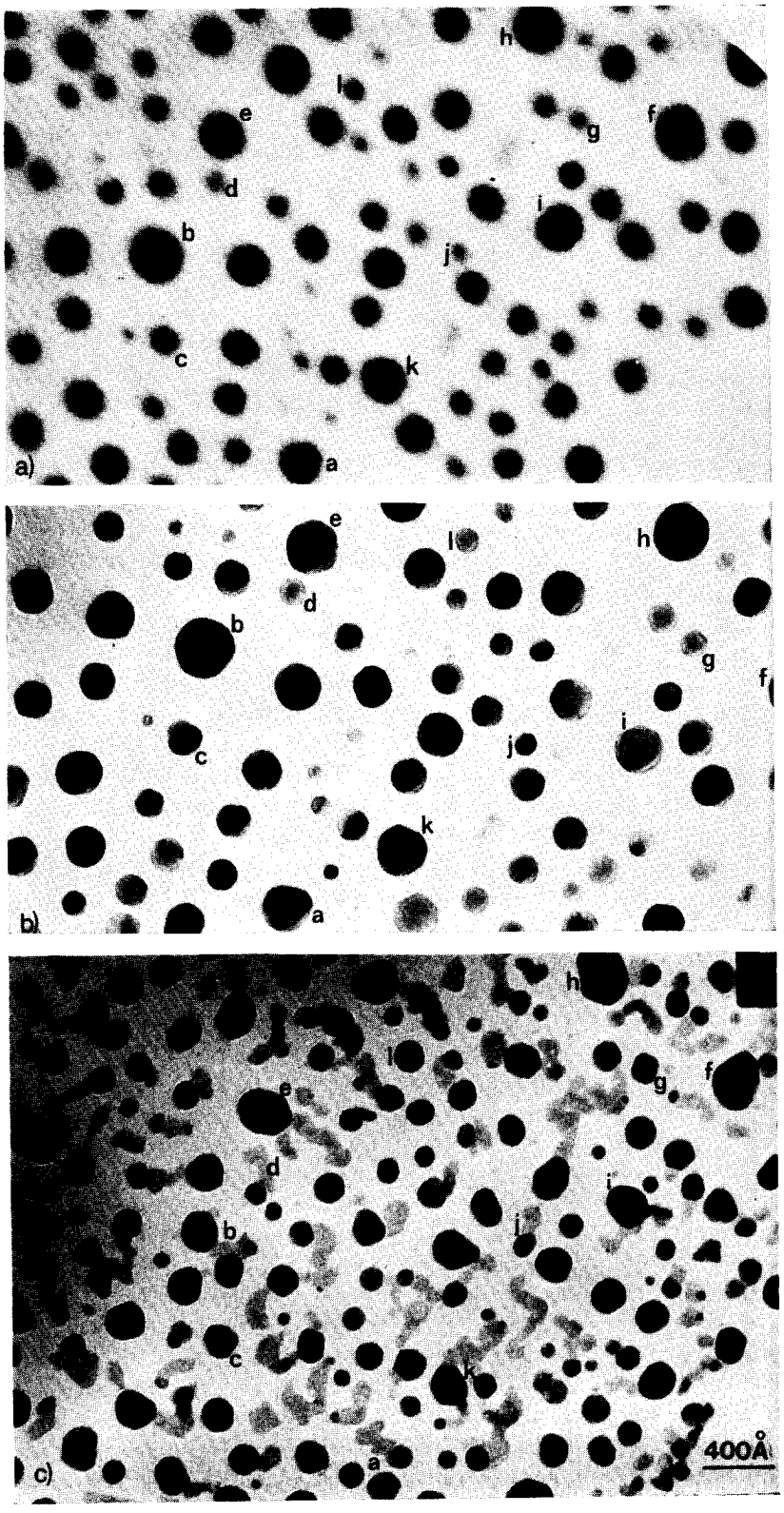
a)
b)
c)
400Å

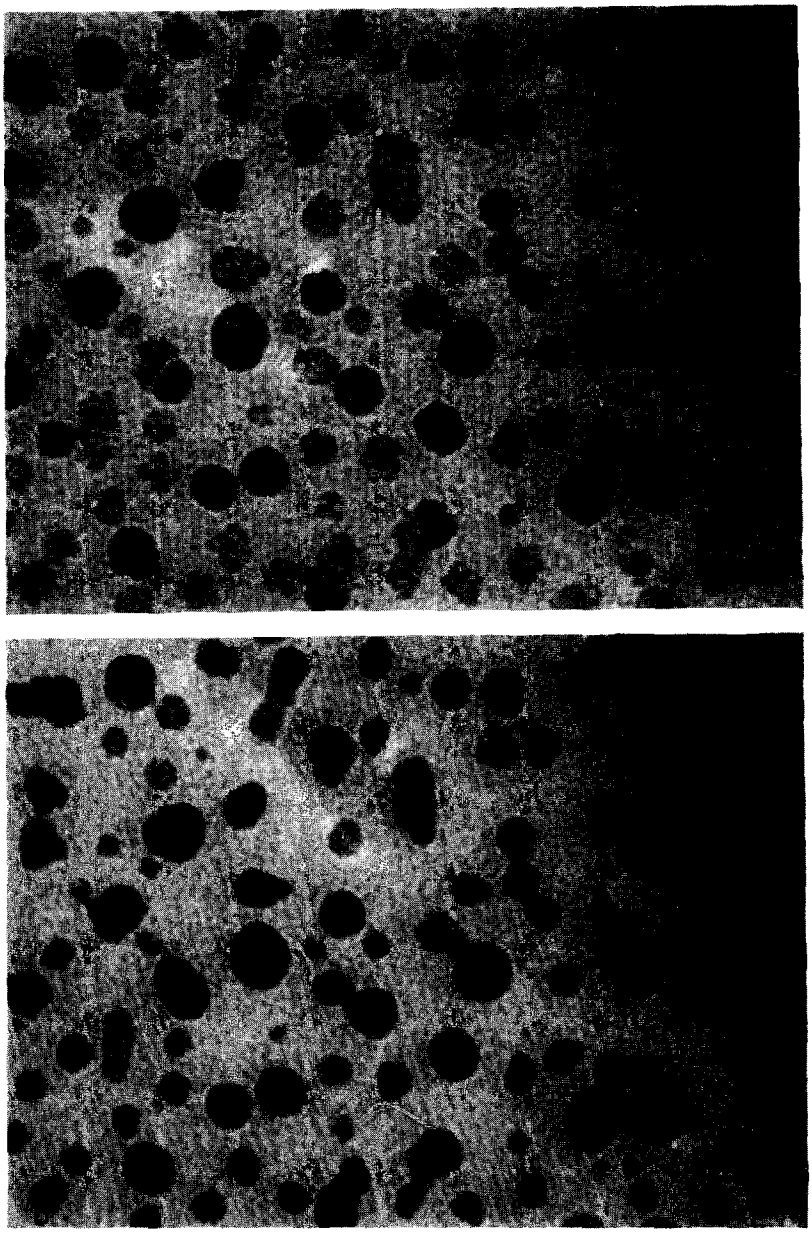

FIG. 9. Micrographs showing H_2 reduction of the oxide on a 50% Pd alloy at room temperature. (a) shows the typical metal and oxide crystallites obtained by heating in air at 650°C while (b) shows the same region after exposure to H_2 at 1 atm for 10 hr at 23°C. After H_2 treatment, diffraction showed only metal, and oxide particles had lost characteristic oxide morphology. Oxide particles also appeared to shrink due to density change and to an increase in height-to-diameter ratio upon reduction to metal.

FIG. 8. Micrographs of a 43% Pd alloy specimen used for X-ray microanalysis. (b) and (c) show TEM micrographs after and before decomposition of the oxide, while (a) shows the STEM image resolution ~15 Å) of the specimen shown in (b). Particles indicated with letters were analyzed for Pt and Pd as shown in Table 1 [(a) and (b) show the images of the sample with 35° tilt].

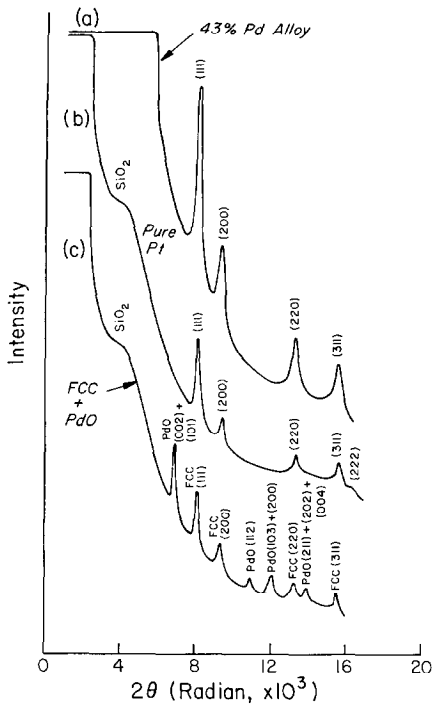

FIG. 10. Typical microdensitometer traces of electron diffraction ring patterns of (a) an alloy heated to 300°C so that only metal forms, (b) pure Pt, and (c) a 43% Pd alloy under conditions where metal and PdO form.

and FCC particles of 50% Pd alloy after heating in air at 615°C are shown in Fig. 12b. Metal particles have a slightly smaller average size but a broader distribution than PdO particles.

The intensity of diffraction peaks is, in principle, proportional to the amount of the corresponding phase present. Thus, the relative amount of PdO and metal on SiO_2 at each temperature could be determined at least qualitatively by the peak intensities of these diffraction lines. Figure 13 shows a plot of areas of a number of diffraction peaks versus heating temperatures for both FCC and PdO. Peak areas were multiplied by appropriate relative structure factors (*18*) for comparison in Fig. 13. Also shown is a sequence with 50% Pd alloys.

As expected the PdO peak intensities increase to about 615°C (the temperature where PdO presumably begins to decompose) and disappears by 740°C. The metal intensities decrease monotonically as metal is converted to oxide and also because layer particles yield lower diffraction intensities.

DISCUSSION

Formation and Decomposition of Oxide

Palladium forms a bulk tetragonal oxide PdO above 400°C which has been reported

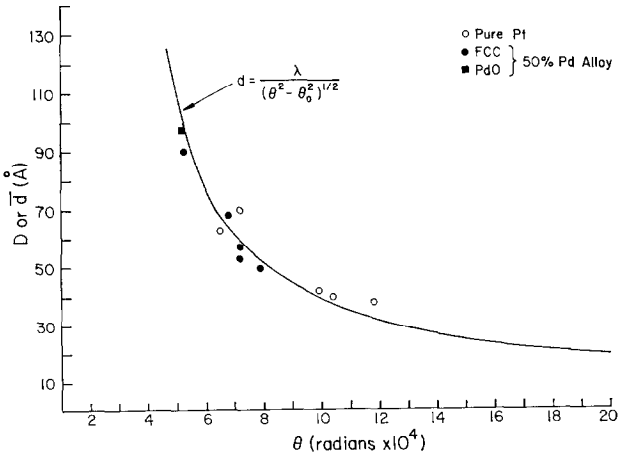

FIG. 11. Plot showing comparison of calculated crystallite size D from Debye–Scherrer equation [Eq. (1)] with the particle diameter $\bar{d}$ measured from micrographs for a number of fcc and PdO diffraction lines. Agreement between geometric and crystalline size is excellent, showing that particles are highly ordered at least down to diameters of ~40 Å.

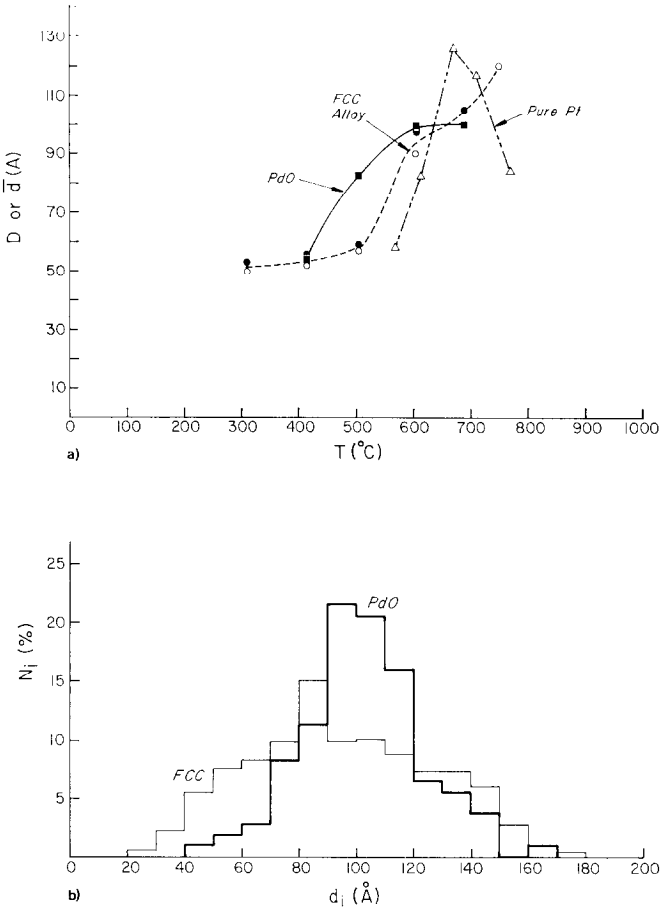

FIG. 12. (a) plot of the diameter D calculated from the diffraction line width using the Debye–Scherrer equation (solid points) or from the average measured size $\bar{d}$ (open points) versus temperature. (b) shows histograms of metal and oxide size distributions for the specimen at 615°C. The oxide has a slightly higher average diameter than the metal, but the distribution is slightly narrower. Data shown for pure Pt are from Ref. (1).

to be stable up to 875°C in 1 atm oxygen and to 700°C in air (*4*). The stability diagram in Fig. 7 shows that a Pd film ~20 Å thick can be oxidized completely as low as 300°C. Figure 7 also shows that the temperatures to form PdO in alloys are composition dependent. Since formation of PdO is controlled by the oxidation rate, it should be temperature, size, and time dependent.

Palladium oxide was observed to disappear at 740°C for a Pd content less than 50%. However, from the observation that PdO diffraction peak intensity decreased for temperature higher than 615°C (Fig. 13), we estimate the onset of decomposition of PdO to be ~650 ± 40°C. Both upper and lower curves in Fig. 7 are composition dependent because both formation and decomposition of PdO are probably limited by kinetics. However, the decomposition onset temperature of PdO is observed to be composition independent from both micrographs and diffraction peak intensity analysis. This result is reasonable since PdO is precipitated out of FCC particles into a presumably pure PdO phase. Thus the activity of PdO should be the same in

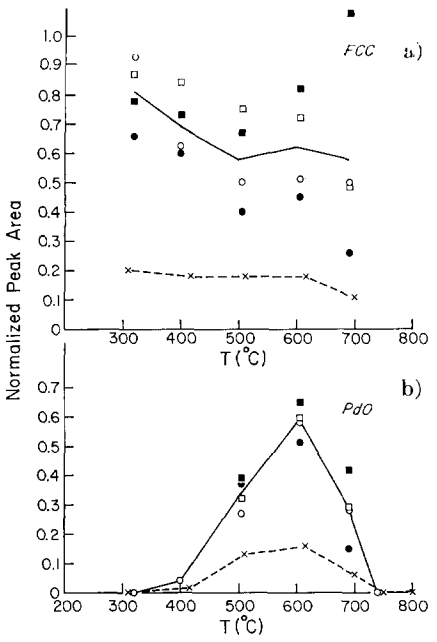

FIG. 13. Diffraction peak areas of (a) metal and (b) oxide for a 50% Pd alloy versus heating temperature in air. The four points at each temperature are from different diffraction lines adjusted by appropriate structure factors. The dashed line shows a specimen with a lower initial metal loading. The metal lines decrease continuously because of loss to oxide and particle growth, while the oxide lines go through a maximum and disappear by 740°C (compare with Fig. 7).

all samples even though the compositions of the starting alloy films are different. The horizontal dashed line in Fig. 7 indicates the decomposition onset temperature of PdO.

Morphology and Interfacial Energy

We observe three different types of morphology of the oxidized alloy as sketched in Fig. 14. For high Pt alloys an oxide phase grows from the side of the metal crystallite (Fig. 14a), for high Pd alloys many small metal crystallites appear at the edges of the oxide particle (Fig. 14b), and for short time, partial oxidation of a thin oxide layer forms on large metal crystallites (Fig. 14c). The identification of metal and oxide is by shape, diffraction pattern, scattering factor, and dark field imaging, although the structures sketched in Fig. 14 should be regarded only as an idealization.

Room temperature H_2 reduction of the oxide particle (Fig. 9) produces a contraction in the size of the particle parallel to the plane of the substrate. The average contraction of oxide area accompanied by H_2 reduction, computed for particles from micrographs of Fig. 9, was 59%. The density decrease between PdO and Pd metal is 68%, and, assuming rectangular parallelopipeds, these numbers predict essentially no change in the thickness (height) of the particle upon reduction from oxide to metal. However, the height to diameter ratio of the particles increases by ~20% upon reduction.

The shapes of metal and oxide crystallites on the SiO_2 substrate are presumably close to those predicted by thermodynamic equilibrium. While the particles are small enough that microscopic effects such as curvature and internal stresses may be significant, it seems reasonable to apply macroscopic thermodynamics incorporating only specific surface free energy or surface tension γ_{ij} for interfaces between phases i and j. The morphologies of Fig. 13 imply that γ between metal and PdO is much higher than that between PdO and SiO_2. The surface tension of Pt in air has been measured to be ~2100 erg/cm² (from grain boundary grooving experiments) (*19*), and γ for glass (*20*) has been reported to be ~1200 erg/cm². The contact angle between

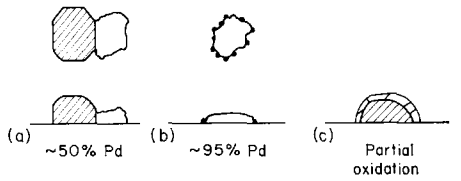

FIG. 14. Illustration of metal and oxide morphologies. (a) shows metal and oxide crystallites for <75% Pd (Figs. 1 and 2a), (b) shows small metal particles at the edges of oxide (Fig. 2b), and (c) shows partial oxidation (Fig. 5).

metal and SiO_2 (*1*) appears to be 90 ± 20° which predicts $\gamma_{M,SiO_2} = 1200 \pm 600$ erg/cm². The lowered height to diameter ratio for PdO implies that $\gamma_{PdO,SiO}$ is much less than this. These are of course only rough estimates, and there is no assurance that even the thermodynamic assumptions are valid. However, it is clear that the interactions between the oxides are much stronger than between metal and oxides.

The strong adhesion of PdO with SiO_2 suggests that there may be significant interdiffusion between phases. Diffraction gives no evidence for paralladium silicates or any other crystalline phases in these experiments. It is reasonable to suppose that the interdiffusion rates in these oxides is too low for much reaction below the 740°C decomposition temperature of PdO.

For small Pd-rich alloys, the formation of many small Pt crystallites on the SiO_2 at the edge of the large PdO particle (Fig. 4b) argues that the interfacial energy between Pt and PdO must be very high because Pt prefers to sit on the SiO_2 rather than on PdO.

Inhibited Evaporation and Sintering

The alloy in O_2 sinters much more slowly than does pure Pt (Fig. 12a), and evaporation of Pt is also reduced (Fig. 6). PtO_2 has a significant vapor pressure while Pd and PdO can be regarded as completely nonvolatile under conditions of these experiments.

The presence of even 8% Pd also inhibits evaporation and sintering of Pt in O_2. The mechanism of Pt sintering has been shown to be exclusively atomic diffusion (*1*), either by metal surface diffusion over the SiO_2 or by vapor transport of PtO_2. Pt and Pd form a complete solid solution, and this suggests nearly ideal solution vapor pressures which would be a large fraction of those of the pure metals. However, it is likely that there is surface segregation of Pd on the crystallite surface, and this could severely inhibit Pt removal from the crystallite. The stability of PdO suggests that in O_2 there should be even more segregation of Pd at the surface, as has been observed for bulk Ni–Au (*6*) alloys.

The overall cause of inhibition of Pt evaporation and sintering by Pd is probably related more to kinetic limitations of Pt volatilization than to thermodynamic limitations. This could arise from a lower Pt density at the crystallite surface where O_2 would react to form PtO_2, or by a reduced rate of escape of Pt atoms to the SiO_2 surface.

SUMMARY

Oxygen has drastic effects on the morphology and sintering properties of Pt–Pd alloys, and the contrast with its effects on pure Pt is quite striking. Most of the observations can be associated with formation and volatilization of Pd and Pt oxides, and with the relative interfacial energies of the phases present. However, they are in no sense predictable from phase diagrams or vapor pressures, and the surface thermodynamics of these systems have not been characterized.

These results show that it is readily possible to produce a separation of this alloy into crystallites containing nearly pure elements by oxidation between 300 and 700°C followed by low temperature reduction of the oxide. It may not be a simple task to produce recombination of separated elements, since the driving force is mainly entropic. The particle size attainable in these systems is smaller (and surface areas are higher) than that in pure metals, presumably because of inhibited growth by oxide formation.

These results have obvious implications regarding the structures of and performance to be expected from alloy catalyst crystallites. The major influences of O_2 treatment and cycling between oxidizing and reducing conditions may be the alterations in morphology and in chemical composition

of individual particles. The oxidizing automotive catalyst consists of Pt–Pd alloys roughly in an atomic ratio of 1:1, and it is clear that in operation the temperature is cycled across the stability boundaries of Fig. 7 and gas compositions are cycled between oxidizing and reducing conditions. There is an almost discontinuous increase in the sintering rate above ~740°C which is associated with the dissociation of PdO; this phase appears to stabilize the crystallites, and rapid crystal growth follows its disappearance. It is easy to envision temperature and gas treatments in this and related alloy catalyst systems which may produce quite specific morphologies, particle sizes, and compositions. In any case, these results point up the inadequacy of simple notions which involve bulk properties and ignore gases, compound formation, and interfacial properties in attempting to explain properties of supported alloy catalysts.

REFERENCES

1. Chen, M., and Schmidt, L. D., *J. Catal.*, submitted for publication.
2. Wynblatt, P., and Gjostein, N. A., *Script. Met.* **7**, 969 (1973).
3. Ducros, R., and Merrill, R. P., *Surface Sci.* **55**, 227 (1976).
4. Samsonov, G. V. (Ed.), "The Oxide Handbook" (C. C. N. Turton and T. I. Turton, transl.), pp. 217 and 397. Plenum, New York, 1973.
5. Lam, Y. L., and Boudart, M., *J. Catal.* **47**, 393 (1977).
6. Palazov, C., Chang, C. C., and Kokes, R. J., *J. Catal.* **36**, 338 (1975).
7. Yamaguchi, S., *J. Catal.* **50**, 541 (1977).
8. Gómez, R., Fuentes, S., Fernánezz Del Valle, F. J., Campero, A., and Ferreria, J. M., *J. Catal.* **38**, 47 (1975).
9. Williams, F. L., and Boudart, M., *J. Catal.* **30**, 438 (1973).
10. Takasu, Y., Shimizu, H., Maru, S., and Matsuda, Y., *Surface Sci.* **61**, 279 (1976).
11. Maire, G., Hilaire, L., Legare, P., Gault, F. G., and O'Cinneide, A., *J. Catal.* **44**, 293 (1976).
12. Norman, J. H., Staley, H. G., and Wayne, E. B., *J. Phys. Chem.* **69**, 1373 (1965).
13. Alcock, C. B., and Hooper, G. W., *Roy. Soc. London, Proc. A* 254 (1960).
14. Boudart, M., and Hwang, H. S., *J. Catal.* **39**, 42 (1975).
15. Kidson, A., *Trans. Amer. Soc. Met.* **58**, 432 (1965).
16. Adams, C. R., Benesi, H. A., Curtie, R. M., and Meisenheimer, R. G., *J. Catal.* **1**, 336 (1962).
17. Dorling, T. A., and Moss, R. L., *J. Catal.* **5**, 111 (1966).
18. X-ray Powder Diffraction Files, 4-0802 and 6-0515.
19. McLean, M., and Hondros, E. D., *J. Mat. Sci.* **6**, 19 (1971).
20. Kaznetsov, V. D., "Surface Energy of Solid," p. 230. Her Majesty's Stationary Office, London, 1957.